Physica Medica 148 (2026) 105859

Contents lists available at ScienceDirect

Physica Medica

journal homepage: www.elsevier.com/locate/ejmp

VIT-MBRT, a GPU accelerated Monte Carlo tool for investigations on preclinical minibeam radiation therapy

N. Luongo [a,b], U. Crimaldi [a,b,f], L.A. Cerbone [a,c,d], X. Jia [e], Y. Lai [e], S. Clemente [b], C. Oliviero [b], R. Pacelli [b,f], A. Spinelli [g], C. Fiorino [h], S. Pizzardi [g], P. Russo [a,d], G. Mettivier [a,d,*]

[a] Istituto Nazionale di Fisica Nucleare, Sezione di Napoli, I-80126 Napoli, Italy
[b] Azienda Ospedaliera Universitaria Policlinico Federico II, I-80131 Napoli, Italy
[c] Scuola Superiore Meridionale, I-80138 Napoli, Italy
[d] Dipartimento di Fisica "Ettore Pancini", Università di Napoli Federico II, I-80126 Napoli, Italy
[e] Department of Radiation Oncology and Molecular Radiation Sciences, Johns Hopkins University, Baltimore MD21287, USA
[f] Dipartimento di Scienze Biomediche Avanzate, Università di Napoli Federico II, I-80131 Napoli, Italy
[g] Centro di Imaging Sperimentale, IRCCS San Raffaele, I-20132 Milano, Italy
[h] Fisica Medica, Ospedale San Raffaele, I-20132 Milano, Italy

ARTICLE INFO

Keywords:
Minibeam radiation therapy
Monte Carlo simulations
TOPAS
GPU

ABSTRACT

Purpose: Minibeam Radiation Therapy (MBRT) is a form of spatially fractionated radiation therapy (SFRT) with electrons, protons, ions or kilovoltage photon beams, aiming to improve the therapeutic window compared to broad-beam irradiation. MBRT with X-rays uses an orthovoltage source and an array of narrow beamlets produced by collimator slits with a typical width of 0.2 mm to 0.7 mm and a center-to-center spacing of 1 to 4 mm. We developed an updated version of *gCTD*, a fast Monte Carlo (MC) code, initially designed for cone-beam CT imaging, to implement a treatment planning system for photon MBRT in mice within a virtual imaging and dosimetry tool (VIT-MBRT).

Methods: We compared *gCTD*, running on a single GPU platform (CUDA environment) with *TOPAS*, a well validated CPU-based simulation code. We simulated irradiation of a water phantom using a multi-slit tungsten collimator with different aperture width and thickness, producing absorbed dose volume data. An example treatment plan was implemented with the *gCTD* code, using a voxelized mouse phantom derived from a CT scan and evaluating organ dose-volume histograms.

Results: Comparison with *TOPAS* simulations showed a good agreement in terms of dose values and peak-to-valley dose ratio (maximum absolute discrepancy of 13% at the phantom entrance surface), with a few percent differences in depth. Simulations with *gCTD* achieved a 300-fold reduction in computational time with respect to corresponding TOPAS simulations.

Conclusions: We realized and validated a fast GPU-based MC simulation code for minibeam radiotherapy, as the basis of the MC platform VIT-MBRT for kilovoltage MBRT preclinical treatments.

1. Introduction

Accelerator-based external beam radiation therapy (RT) with megavoltage X-rays employs multiple broad beams to irradiate the target volume, aiming to maximize tumour control while minimizing complications to normal tissues. In conventional RT, this is achieved by focusing the radiation dose on the tumour volume through irradiation with fields from multiple views, while sparing organs at risk by spatially constraining the dose delivered to surrounding healthy tissues. However, recent studies have shown that the therapeutic window can be further enhanced through novel techniques such as temporally fractionated FLASH radiotherapy, which uses ultra-high dose rates, as well as the microbeam radiation therapy (MRT) and minibeam radiation therapy (MBRT). These latter methods belong to the broader class of spatially fractionated radiation therapy (SFRT) techniques, in which the broad beam of conventional RT is replaced by a spatially modulated beam incident on the patient and propagating through tissues, typically in the form of quasi-parallel laminar beamlets.

* Corresponding author at: Dipartimento di Fisica "Ettore Pancini", Università di Napoli Federico II, I-80126 Napoli, Italy.
E-mail address: mettivier@na.infn.it (G. Mettivier).

https://doi.org/10.1016/j.ejmp.2026.105859
Received 31 October 2025; Received in revised form 4 May 2026; Accepted 13 June 2026
Available online 28 June 2026

MRT was first investigated in the 1990s at Brookhaven National Laboratory [1,2], and subsequently developed at the European Synchrotron Radiation Facility (ESRF) [3] and the Australian Synchrotron [4]. MRT involves spatially fractionated high-dose-rate (mono- or polyenergetic) low-energy photon irradiation (e.g., 40–290 keV at ESRF). The beam is quasi-parallel and non-homogeneous, consisting of alternating high- and low-dose regions, referred to as "peaks" and "valleys", respectively. As a result, both tumour and healthy tissues are irradiated by an array of beams a few tens of micrometres wide, delivering unconventionally high doses (100–1000 Gy) in a conformal treatment [5]. The peak dose is maximized at the central region of each planar beam, while the valley dose is minimized. The peak-to-valley dose ratio (PVDR) represents the key dosimetric parameter used to evaluate the quality of spatially fractionated radiation therapy. The dose difference between the peaks and the valleys can reach thousands of grays over micrometre-scale distances, but an ideal energy for clinical MRT has not yet been established [6]. Shinohara et al. recommend an energy range of 90–300 keV for treating deep-seated tumours, depending on the application and irradiation geometry [7–9]. Prezado et al. suggested an energy of 175 keV [10], whereas Livingston et al. identified the best energy range between 90 and 120 keV [7].

In recent years, the MRT approach has been successfully adopted in preclinical research. However, the required high doses and dose rates can currently be achieved only with synchrotron x-ray sources and, currently, there are only a few MRT facilities worldwide, such as the ESRF in France and the National Synchrotron Light Source, Brookhaven National Laboratory in the United States capable of achieving such performance [11].

Recent advancements in preclinical radiation therapy research aim to bridge the gap with clinical treatments by improving experimental comparability. Modern small-animal irradiators now incorporate image guidance and adaptive treatment planning [2]. Given these advantages, orthovoltage X-ray MBRT represents a promising cost-effective alternative to MRT for preclinical treatments. This technique, based on the use of X-ray tubes and beam widths of hundreds of micrometers, is currently under investigation at several centers for preclinical research. As part of a Next Generation EU project—PNRR-Sanità proof-of-concept project, partners: San Raffaele Hospital (Milan, Italy); Polyclinic and University Federico II (Naples, Italy)—we are investigating preclinical MBRT for spatially fractionated radiation therapy (SFRT) using a 225 kVp X-ray irradiator, through Monte Carlo (MC) simulations and in-vivo experiments on mice. The study aims to optimize geometrical and dosimetric parameters for both planar irradiations (with various MBRT collimators) and full rotational irradiations around the target [12–14].

Key aspects of computational modelling include accuracy and simulation time. General-purpose MC codes (full-MC) running on CPU-based hardware can provide accurate and precise dose estimates, but they often require extensive computation time, especially when the number of simulated primary photons is large (10^{10}–10^{12} primaries, or higher), which is necessary for obtaining reliable statistics and direct comparison of simulated dose values with actual absorbed doses in the target.

To address this limitation, in this work we devised a MC simulation platform (called VIT-MBRT) based on a new version (v1.2) of *gCTD*, a GPU-based MC code, originally developed in 2011 for cone-beam CT in radiotherapy [15,16]. *gCTD* v1.1 was previously validated for low energy photons up to 150 keV [17]; the new version (v1.2) extended its range to 350 keV photon energy. This MC platform allows for replicating the irradiation geometry of the physical apparatus and scoring the absorbed dose distribution within a digital phantom of the mouse, given as input to the simulation. The code includes a digital replica of the preclinical irradiator, modeling both the X-ray output and irradiation geometry, and computing the 3D absorbed dose distribution within the digital phantom. In this work, we implemented an updated version incorporating energy-dependent cross sections up to 350 keV, enabling its use in MBRT simulations. This required the introduction of new attenuation coefficients and, consequently, a new validation procedure. We validated the *gCTD* v1.2 code through direct comparison with the well-established *TOPAS* code (based on the Geant4 simulation toolkit) evaluating 3D dose profiles in all media downstream of the X-ray tube.

2. Materials and methods

2.1. GPU-based code

The originary *gCTD* v1.0 GPU-based dose calculation code [15,16] is a MC simulation tool originally developed at the University of Texas Southwestern Medical Center (suppl. materials, tab. S1). In this code, developed using CUDA version 11.6 for GPU computing, the photon transport is modelled using the Woodcock tracking method [18], which improves computational efficiency of the boundary crossing process. The code accounts for Compton scattering, Rayleigh scattering, and photoelectric absorption. Photons continue to propagate until their energy drops to 1 keV or they exit the phantom. It is important to note that *gCTD* does not simulate electron transport: secondary electron deposit their energy locally, i.e. in the voxel where they are generated. This approximation—which permits a drastic reduction in computation times—is considered acceptable if the voxel size is larger than the electron range. For instance, according to the NIST ESTAR database, the continuous slowing down approximation (CSDA) range of 87 keV electrons in water is about 100 μm, i.e. less than the voxel size (100 μm by side) [19]. The absorbed dose in each voxel of the simulated material bulk is computed as the total energy (in eV) deposited by photons and secondary electrons, divided by the voxel mass (in grams), and then scored in microgray (μGy). A complete description of the original code is reported in [15,16]. In this work, starting from a previous version v1.1 [20], we developed the version 1.2 of the *gCTD* code, by extending the cross-section dataset to 350 keV photon energy. *gCTD* v1.2 runs on a GPU card type NVIDIA GeForce RTX 3090Ti (10496 cores, clock speed 1.70 GHz and 24 GB of dedicated GDDR6X memory), under the CUDA version 11.6 programming environment (CUDA 2023). *gCTD* v1.1 was previously tested following the AAPM TG-195 report (case 1) and a direct comparison with the Geant4 MC code [17,21].

2.2. TOPAS code

The validation of the VIT-MBRT platform was carried out by comparing the *gCTD* code with the *TOPAS 3.9* code (suppl. materials, tab. S2), previously validated through dosimetric measurements at IRCCS San Raffaele Hospital, in Milan [12–14]. *TOPAS* (Tool for particle simulation, https://topasmc.org) version 3.9 is an extension of Geant4 toolbox (version 10.5.p01), widely used in physics, biology and clinical research. It provides a user-friendly interface that reduces setup errors (e.g., unit mismatches or scoring inconsistencies) and allows reproducible simulations by enabling restoration of prior configurations [22]. *TOPAS* can model many type of particles, such as electrons, photons, protons and heavy ions and simulate their path through the matter in several complex geometries, including medical instruments, detector and patients (the patient can be imported in a DICOM format or others). During the particles transport Compton scattering, gamma conversion, photoelectric effect for photons, multiple scattering, and ionization are simulated. The physics list used in TOPAS application was built with the Geant4_Modular option using modules recommended for kilovoltage radiotherapy applications (g4em-livermore, g4h-phy_QGSP_BIC_HP, g4decay, g4ion-binarycascade, g4h-elastic_HP and g4stopping). A range cut of 0.100 mm was used in all cases and for all particle types. The code ran on a computer server embodying two AMD EPYC 7281, 2.2 GHz, 32-core processors, 256 GB RAM.

2.3. Setup description

Simulations reproduced the geometry of a dedicated small animal

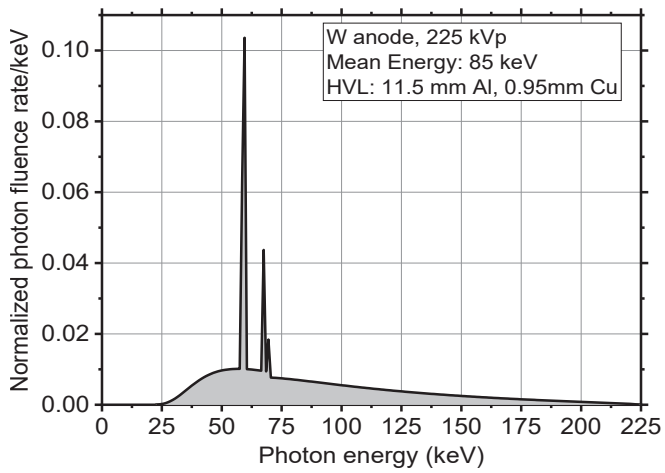

Fig. 1. X-ray spectrum (W anode, 225 kVp, 2 mm Be, 0.3 mm Cu filtration) used for simulations with both TOPAS and gCTD code, generated with the SpekCalc code [23].

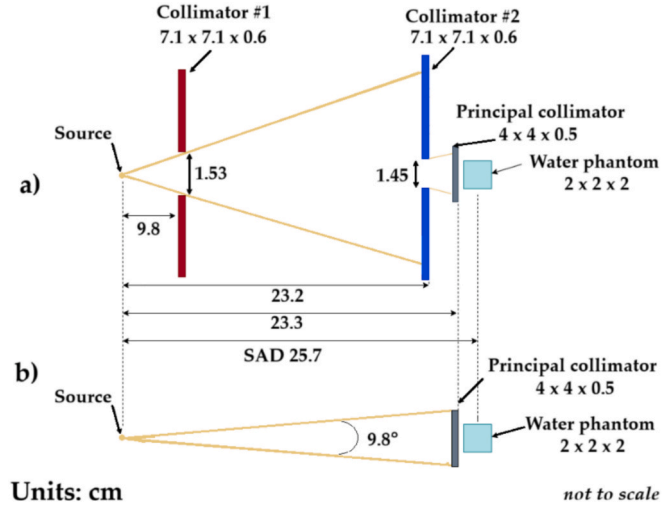

Fig. 2. Sketches of the simulated setup geometry in a) TOPAS, and b) in the gCTD simulation codes.

irradiator (X-RAD225Cx SmART, Precision X-ray, North Branford, CT, USA), equipped with an orthovoltage 225 kVp X-ray tube with a tungsten anode and a dual focal spot (for treatment or imaging mode, respectively). The system is mounted on a rotational C-arm gantry, used for preclinical treatments at the Preclinical Imaging Facility of San Raffaele Scientific Institute. We simulated a 225 kVp spectrum with 2 mm Be inherent filtration and 0.3 mm Cu additional filtration, and a 3.5 mm diameter focal spot. Fig. 1 shows the X-ray spectrum, used for both *TOPAS* and *gCTD*, generated using the SpekCalc code [23].

We simulated the irradiation of a voxelized cubic water phantom (volume, $2 \times 2 \times 2$ cm^3, $0.1 \times 0.1 \times 0.1$ mm^3 voxel size) positioned at 25.7 cm from the X-ray source (Fig. 2). We analysed the 3D absorbed dose maps in the water phantom, with transverse dose profile consisting of a series of high-dose regions (*peaks*) alternating with low-dose regions (*valleys*), characterized by a high *PVDR*. The peak and valley doses, as well as the *PVDR*, were evaluated at different depths. We first simulated an open beam irradiation (no collimator) and then added a multi slit collimator (principal collimator) in front of the target, at 23.3 cm from the source (Fig. 2) to simulate a minibeam irradiation geometry. In *TOPAS*, before reaching the main collimator, the beam passed through two lead pre-collimators. The pre-collimators were $7.1 \times 7.1 \times 0.6$ cm^3 lead collimators positioned at 9.8 cm and at 23.2 cm from the source and with an aperture of 1.53×1.53 and 1.45×1.45 cm^2, respectively, reducing the divergence of the beam to 3°; the dimensions of the beam reaching the principal collimator were 1.5×1.5 cm^2.

In *gCTD*, the X-ray beam existing the focal spot was simulated with a circular shape of 4 cm diameter, and a divergence angle of 9.8° (Fig. 2b). The principal collimator and the water phantom, as in *TOPAS*, were placed at 23.3 cm and 25.7 cm from the source, respectively. The simulated geometry is reported in Fig. 2b.

2.4. Code comparison validation

To validate the *gCTD* v1.2 code, we carried out a series of tests in which different quantities were measured, and different radiation geometries were implemented:

- *Half value layer (HVL):* An important parameter to characterize the X-ray beam is the HVL. The geometry was realized in order to have a 50 cm distance from source to the detector, while the beam angle was reduced to 0.5° that ensures a good geometry to calculate the HVL. A first simulation was done without any filter at the output of the tube, and then, by adding a 3×3 cm^2 Cu or Al filter, with the expected HVL thickness (0.95 mm Au and 11.5 mm Al, respectively [24]).We estimated the HVL of the simulated spectrum using both codes, for a monoenergetic (85 keV) photon beam. To this end, we calculated the photon fluence in air at 50 cm from the source, with and then without adding an aluminium or copper filtration.
- *Monoenergetic beam*: We simulated an open beam irradiation with a monoenergetic beam with energies of 85 and 225 keV, which are equivalent to the average and maximum energy of the X-ray irradiator spectrum, respectively. The simulations were carried out as in open field configuration by scoring 2×10^{10} photons. The dose distributions were simulated in the water cube (Fig. 2) without the principal collimator. In *gCTD* geometry, a tungsten cover with a single 1.5×1.5 cm^2 slot was designed to preserve the beam's dimensions. The dose value was estimated using the ImageJ software tool [25] as the mean value in a region of interest (ROI) of 50×50 voxels at the centre of each slab of the simulated water volume (Fig. 6). A comparison between the estimated percentage depth dose (PDD) of the two codes was performed.
- *Polychromatic beam*: Using the same configuration as for the monoenergetic beam, a comparison between the estimated PDD of the two codes was realized using the X-ray irradiator spectrum. In this case 10^{11} primary photons were launched.
- *Mass attenuation coefficient:* To ensure a correct modelling of the materials in the *gCTD* simulation code, we compared the mass attenuation coefficient of tungsten at 85 keV. This was done by adding a 1 mm tungsten slab in the configuration used for monoenergetic beam, and the mass attenuation coefficient of tungsten was calculated with *gCTD* code. We simulated a 0.5° aperture beam of monoenergetic 85 keV photons. In this case 1×10^{12} primary photons were simulated, and the value was compared with that reported by NIST [24].
- *Multi Slit collimator*: We modelled the principal collimator as a tungsten slab of 4×4 cm^2 with parallel slits. The slits are oriented perpendicular to beam axis, with a fixed center to center (c-t-c) of 1 mm and dimensions ranging from 0.1 to 0.5 mm. The thickness varies from 1 to 5 mm. In these cases, 2×10^{10} primary photons were simulated. Dose values were measured as the average value in a 2×80 pixels ROI in the peak and in the valley as indicated in Fig. 8c (ROIs in red colour).

2.5. Experimental validation

The experimental validation was carried out at San Raffaele Hospital (Milan, Italy) by comparing simulated and measured doses in a PMMA phantom. The phantom consisted of a PMMA cube ($50 \times 50 \times 21.2$

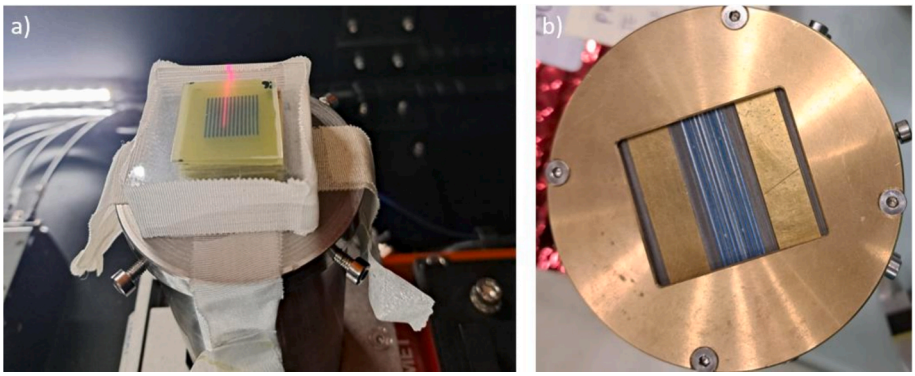

Fig. 3. (a) Photo of the PMMA stacked phantom with radiochromic film inserts, irradiated by MBRT treatment; (b) photo of the stacked 5 mm-thick tungsten/polypropylene collimator, with 0.5 mm aperture slits and 1 mm c-t-c spacing.

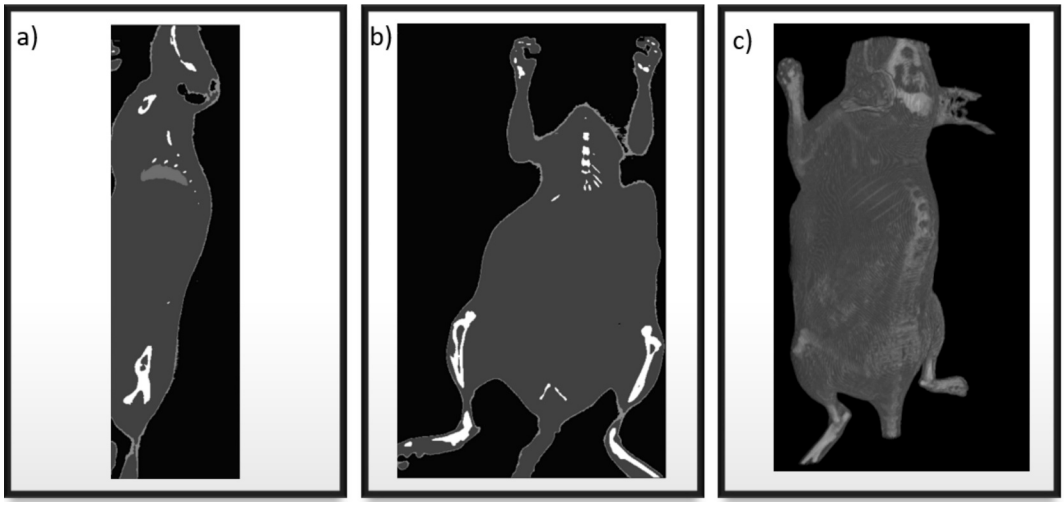

Fig. 4. Voxelized phantom of a mouse obtained from the segmentation of a CT mouse scan in (a) central sagittal slice, (b) central coronal slice, and (c) 3D view.

Table 1
Simulated attenuation I/I_0 calculated with TOPAS and gCTD codes, using the HVL values (in Cu and Al) calculated by the SpekCalc software, for the 225 kVp spectrum of the X-RAD225Cx irradiator.

SpekCalc value		Simulated I/I_0
HVL 0.95 mm Cu	*gCTD*	0.489
	TOPAS	0.496
HVL 11.5 mm Al	*gCTD*	0.488
	TOPAS	0.515

mm^3) composed of ten stacked 50 × 50 × 2.12 mm^3 PMMA slabs. Every 2 slabs, a 2 × 2 cm^2 piece of EBT3 radiochromic film (Ashland, Inc., USA), previously calibrated, was placed so to determine the absorbed dose at six different depths in the PMMA phantom (Fig. 3a). The MBRT collimator used for experimental tests was made of tungsten (Fig. 3b), with a thickness of 5 mm and parallel slits of 0.5 mm aperture and 1 mm c-t-c spacing.

The radiochromic films were then scanned using an Epson Expression 12000XL flatbed scanner, in transmission mode, at 400 dpi resolution. We analysed the scanned images using the FilmQApro software (Ashland, Inc., USA), following a triple-channel (blue, green, red) dosimetry protocol. The measured dose in the PMMA stacked phantom was then compared with that obtained from simulations with *TOPAS* and *gCTD* codes (2 × 10^{10} primary photon histories launched in the simulations).

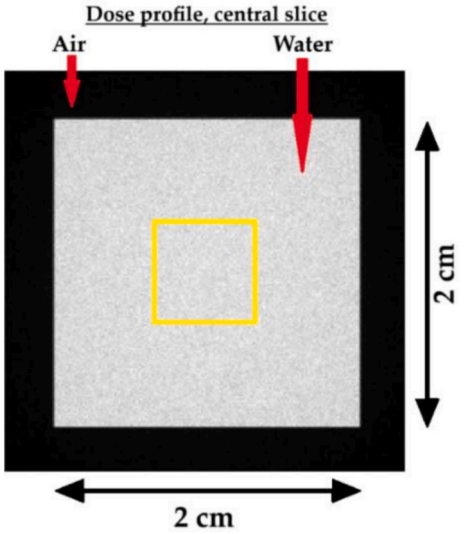

Fig. 5. Example of the dose distribution at the central plane of a water cube when irradiated without the principal collimator (open field simulation set up). The yellow square box indicates the centered ROI of 0.5 × 0.5 cm^2 in the central slice of the phantom, used to measure the average dose in each depth slice. (For interpretation of the references to colour in this figure legend, the reader is referred to the web version of this article.)

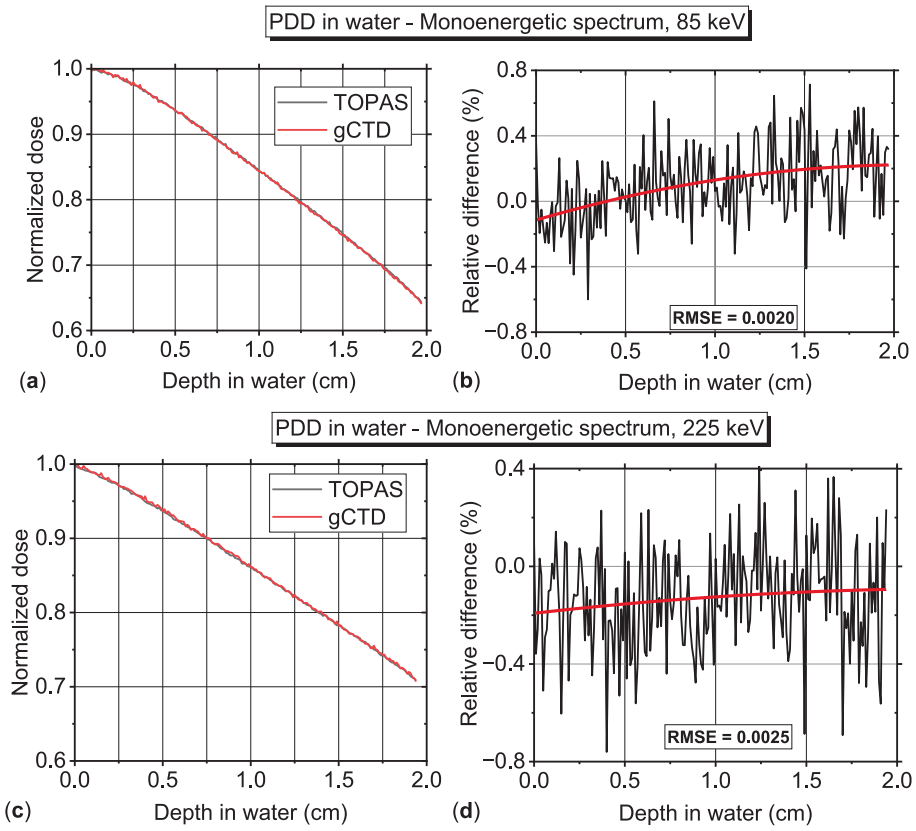

Fig. 6. Normalized dose as a function of depth in a $2 \times 2 \times 2$ cm^3 water phantom, irradiated with a monoenergetic beam (a) at 85 keV and (c) at 225 keV, using both *TOPAS* and *gCTD*; corresponding relative differences are shown in panel (b) and (d).

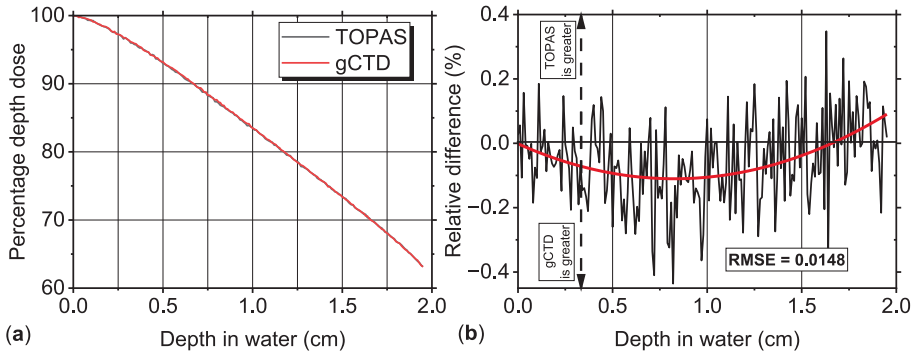

Fig. 7. A) comparison between the percentage depth dose curve in water, as simulated with *TOPAS* (black line) and with *gCTD* (red line). b) Relative difference between the two trends in (a), vs. depth, calculated as 100* (topas-gctd)/topas; the root mean square error is reported, and the red horizontal line indicates the relative average difference. (For interpretation of the references to colour in this figure legend, the reader is referred to the web version of this article.)

2.6. Simulation of the MBRT treatment of a mouse

Finally, we simulated the irradiation of a tumour-bearing mouse with an MBRT preclinical treatment. The voxelized phantom of the mouse was obtained by segmenting the mouse organs (body, bone, skin, lung and heart) in a computed tomography (CT) dataset of a mouse previously MBRT-treated at San Raffaele Hospital. The CT scan was obtained with the imaging unit of the X-RAD225Cx irradiator. The voxelized mouse phantom (voxel size, $0.1 \times 0.1 \times 0.1$ mm^3) was incorporated into the *gCTD* geometry (Fig. 4). We performed a simulation both with the open beam and with the MBRT configuration. For the MBRT treatment we compared the *gCTD* virtual dosimetry data with the preclinical treatment data of the treatment planning system (TPS) of the X-RAD225Cx irradiator, while for the open beam preclinical irradiation the comparison was made with a simulation in *TOPAS*. As many as 10^{11} primary photons were simulated in the open beam, and 10^{10} primaries in the MBRT simulation. A 4 mm-diameter spherical mask was created and applied to the 2D dose image, to evaluate the dose absorbed in the tumour volume. Simulated dose values were then rescaled to have an average dose of 15 Gy to the tumour (the preclinical treatment target dose). Moreover, to study the dosimetry in the tumoral tissue and the surrounding healthy tissues, 10^{12} photons were simulated in *gCTD* code and dose-volume histograms were then generated, using different masks applied to each organ at risk.

To assess the statistical uncertainty of the MC simulation, we repeated ten times the simulation used for the dose calibration (batch method, [26]). For each simulation we derived the mean value and the standard deviation of the mean of the ten repetitions. The standard

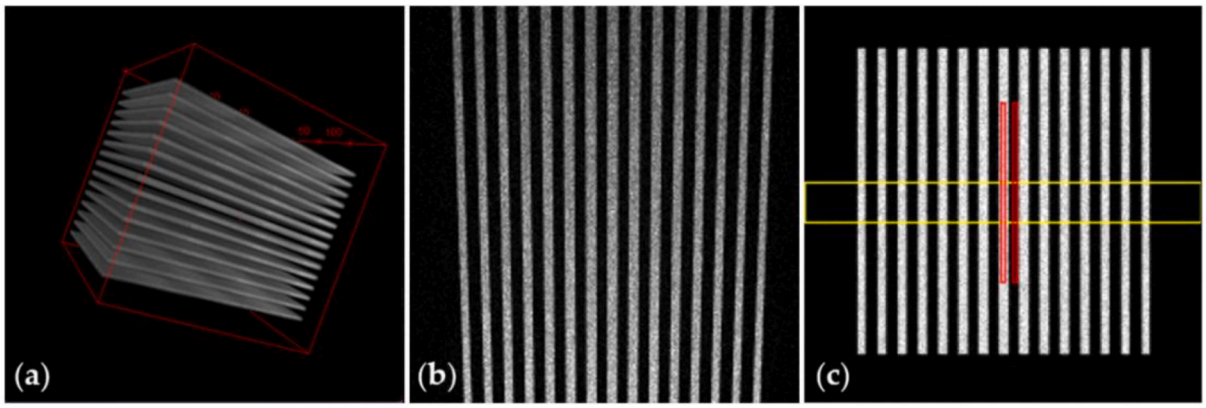

Fig. 8. An example of the expected a) 3D dose distribution in the water phantom and the corresponding 2D dose distribution b)in the coronal plane, and c) in the axial plane.

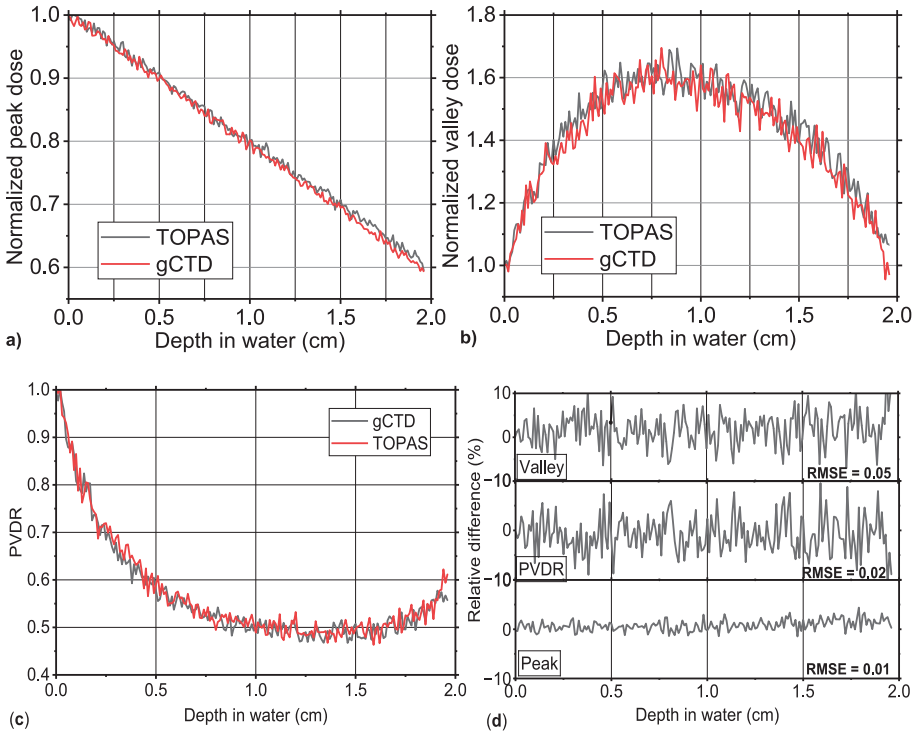

Fig. 9. Plot of normalized dose in the peak (a), the valley area (b) and relative *PVDR* value, respectively. The relative differences between the two codes are shown in (d). Simulated data were obtained using a tungsten parallel collimator with 0.5 mm aperture.

deviation of the mean divided by the mean of the ten repetitions was reported as the statistical uncertainty on the simulations results (0.05%).

3. Results

3.1. Half value layer (HVL)

To verify the accuracy of the code, we evaluated the attenuation of the beam intensity (I/I_0) using aluminum (Al) or copper (Cu) filters with a thickness equal to the HVL value of the X-RAD225Cx SmART spectrum (Fig. 1). The HVL, calculated through SpekCalc is 11.5 mm Al or 0.95 mm Cu. In order to verify this value, 2×10^{10} photons were set for each simulation in both simulation codes. The results are reported in Table 1. The difference between the observed value (simulated attenuation I/I_0 in Tab. 1) and the expected value ($I/I_0 = 0.500$) is at most 3%, while the relative differences between the two codes are 1.4% and 5.5% respectively for Cu and Al filters.

3.2. Monoenergetic beam

The $2 \times 2 \times 2$ cm^3 water phantom was irradiated with a monoenergetic beam, with an energy value of 85 keV or 225 keV. For each simulation 2×10^{10} photons were scored and the average value in a central ROI of 0.5×0.5 cm^2 was measured (yellow square ROI in Fig. 5). The normalized dose vs the depth was then plotted for both the codes and for both the energies (Fig. 6). A relative difference and an RMSE less than 0.3% and 0.003, respectively, were measured.

3.2.1. Mass attenuation coefficient in tungsten

We measured the beam attenuation in a slab of tungsten (density $\rho = 19.25$ g/cm^3) to determine the attenuation coefficient at 85 keV. For this test we calculated the mass attenuation coefficient using a

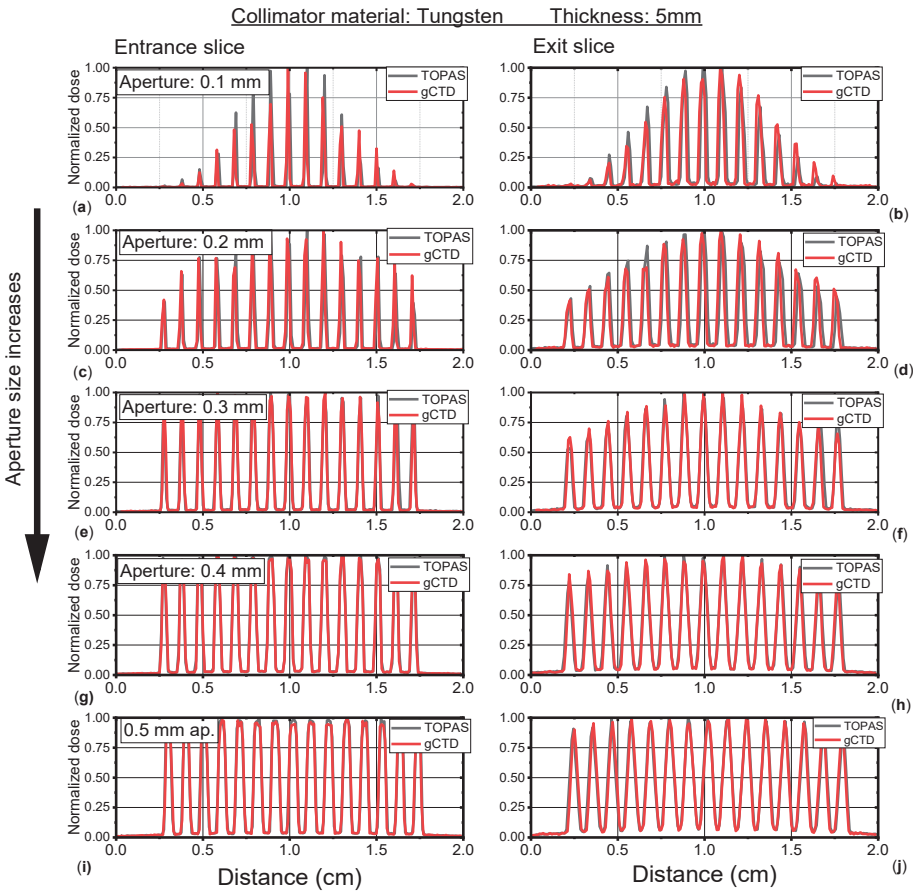

Fig. 10. Dose profile evaluated at the entrance (left column) and exit surface (right column), respectively, simulated using tungsten/air minibeam collimators, with open aperture varied from 0.1 mm to 0.5 mm.

monoenergetic beam, with an energy of 85 keV and a tungsten slab (thickness, $t = 1$ mm), launching as many as 10^{12} photons in the simulation. Using narrow-beam geometry, we estimated the attenuation coefficient from the Lambert-Beer law: $\mu = \left[-\ln\left(\frac{I}{I_0}\right)/t\right]$. The corresponding mass attenuation coefficient μ/ρ was then compared with the expected value (6.778 cm^2/g) for pure tungsten at 85 keV, as reported by NIST [23]. We obtained a value of $\mu/\rho = 6.570 \pm 0.225$ cm^2/g, which agrees (within 3%) with the expected value, considering the statistical uncertainty (3%) in the simulation.

3.3. Percentage depth dose in water

For this test, we used the irradiation setup described in section 2.4. For both codes, 10^{11} primary photons were simulated. Fig. 7a shows the PDD measured in a 50 × 50 pixel ROI in a slice at the centre of the water phantom (Fig. 5), for both simulation codes. In Fig. 7b, the relative difference between the data obtained with the two simulation codes was plotted, showing an average percentage difference of about 0.1% and a RMSE of 0.00148.

3.4. Multi slit collimator

Fig. 8 shows an example of the 3D dose distribution (Fig. 8a), as well as the 2D dose distributions in the coronal (Fig. 8b) and axial planes (Fig. 8c) of the simulated water cube, obtained from both simulation processes. This dose distribution was achieved using the principal collimator described in section 2.4, with slits oriented perpendicular to the beam axis. The collimator material was tungsten, and simulations with different slabs' aperture were made, from 0.1 mm to 0.5 mm in a 1 mm step. Dose values in the peak and in the valley were extrapolated to compare the *PVDR* as a function of the depth in the simulated water cube obtained by the two codes. Dose profiles were plotted along the yellow ROI (200 × 20 pixels) shown in the same figure. All simulations were carried out launching 2 × 10^{10} photon histories, and the corresponding dose distributions were normalized to their respective maximum dose values.

3.4.1. Collimator with a fixed thickness

A 200 × 20 pixel ROI was tracked like in the previous case (Fig. 8c, yellow ROI). Fig. 9 shows the results of the normalized doses in depth in the irradiated (Fig. 9a), in the shaded zones (Fig. 9b) and the *PVDR* (Fig. 9c), while the dose profiles at the surface and in the depth of the target were reported for the five different apertures in Fig. 10. Fig. 9d shows the relative difference between the peak dose, valley dose and *PVDR* obtained with the two codes. From this figure it is possible to note that the fluctuations in the difference of *PVDR* with the two codes are due mainly to the fluctuations in the valley dose, where the photon statistics is low. In each case the *PVDR* was calculated by tracking a 2 × 80 pixel ROI at the center of the cube (Fig. 8c, ROI in red colour). The values were then plotted, with the relative differences between *TOPAS* and *gCTD* codes (Fig. 11). The percentage error between the two codes, on the average, remains between 2% and 5%, except in cases of minimal aperture (0.1 mm), where it reaches a maximum of +13% (*gCTD* underestimation) at the entrance surface of the phantom.

3.4.2. Collimator with a fixed aperture

We simulated a collimator with a fixed aperture (0.3 mm) and varying thickness from 1 to 5 mm. The *PVDR* was calculated tracking a 2 × 80 pixels ROI (Fig. 8c, ROI coloured in red) and then plotted with the

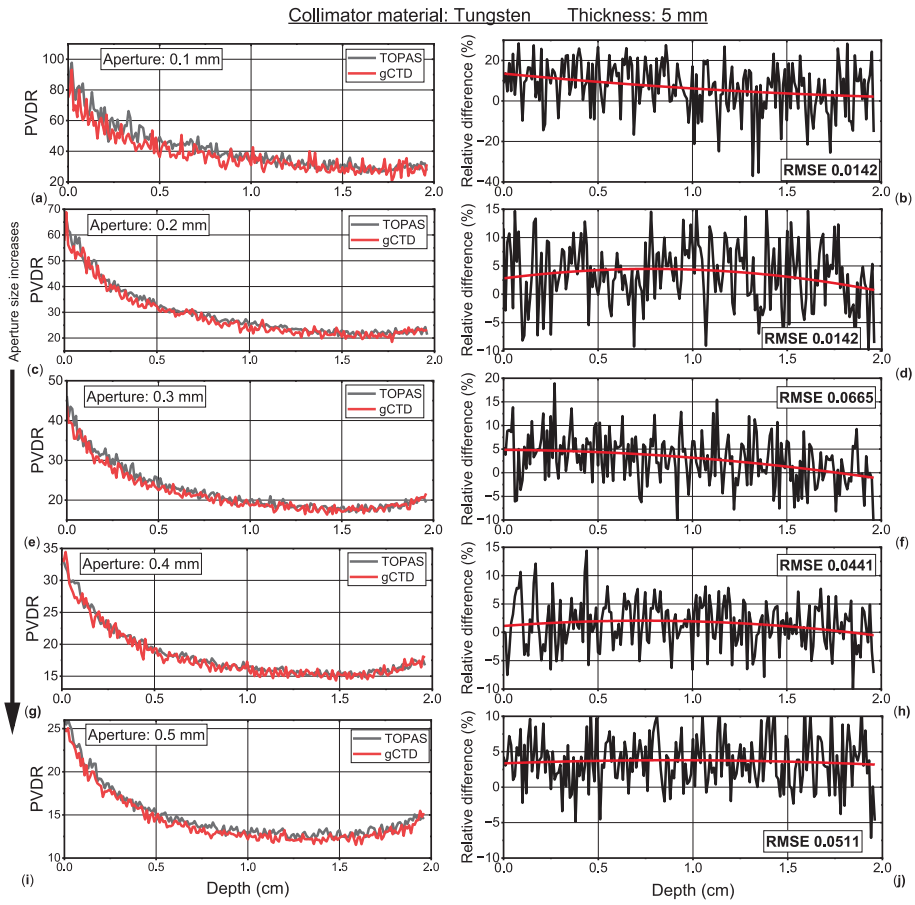

Fig. 11. (Left column, panels a), c), e), g), i)): Comparison of *PVDR* at the center of the water cube, in the case of a tungsten parallel collimator with varying aperture from 0.1 mm to 0.5 mm, calculated with *TOPAS* and *gCTD*. (Right column, panels b), d), f), h), j)): Percentage relative difference between values provided by *TOPAS* and *gCTD* codes in corresponding left-column plots; the continuous red line shows a moving average smoothed trend of the data shown by the continuous black line. (For interpretation of the references to colour in this figure legend, the reader is referred to the web version of this article.)

relative difference between the two codes (Fig. 12). The maximum percentage error ranges within ±10% on the average, with a maximum deviation of −13% (*gCTD* overestimates) at the entrance surface of the phantom (Fig. 12c,d).

3.5. Experimental validation

In this test, we compared the two codes with experimental data. The test was carried out to validate the peak dose and the *PVDR* values. We irradiated a PMMA stacked phantom, prepared as described in section 2.5. This phantom was irradiated with the preclinical unit (225 kVp, 30 mA, 90 s exposure time). The experimental data were compared with the simulated ones. Fig. 13a shows the experimental profile vs. the simulated data (both *gCTD* and *TOPAS* codes). In both cases a similar trend is observed, although air was used as the inter-slab material in the simulation, while the experimental collimator employs polypropylene, which was not available in the material libraries of the *gCTD* code.

The comparison of the peak dose values, shown in Fig. 13b, points out an average relative difference of 2% with *gCTD* code and 3% with *TOPAS* code, while for the *PVDR* vs. depth (Fig. 13c), one observes a 0.05% average relative difference with *gCTD* and 3% with *TOPAS*.

3.6. Mouse phantom

MC simulations were run using the mouse voxelized phantom (Fig. 4). Fig. 14 shows the simulation with the *gCTD* code for irradiating the mouse in the open beam geometry (Fig. 14a) and with a MBRT geometry (5-mm-thick tungsten parallel collimator with an aperture of 0.5 mm) (Fig. 14c). The open beam simulated dose map was compared with the preclinical dose map calculated with the available irradiatior's TPS (Fig. 14b), while the MBRT simulation was compared with that obtained with the *TOPAS* code (Fig. 14d). The dose-volume histograms (DVHs) in the tumour for both configurations (Fig. 15) were obtained using a 4 mm-diameter spherical mask outline the tumour in sliced dose maps, as shown in Fig. 4.

Fig. 16 shows the dose-volume histograms for tumour and for all segmented organs at risks, for the open beam (Fig. 16a) and MBRT (Fig. 16b) geometry, respectively obtained using the *gCTD* simulation code.

4. Discussion

MC simulations are becoming increasingly popular in minibeam radiotherapy research, as they help reducing the ethical and economic burden associated with animal and clinical experiments. In this scenario, computation time is a crucial factor in a virtual experiment, where lengthy code tests and validation tests are necessary, multiple configurations may need to be tested to identify the most suitable one for clinical translation, and realistic virtual dose values (1 − 100 Gy to the target) should be produced for the 3D dose maps, in a (preclinical) treatment planning system. CPU-based full-MC codes are known for their high accuracy but are also computationally intensive, often requiring lengthy time periods to complete simulations involving large number of photons needed to achieve reliable statistics. In this work, we introduced a new GPU based MC simulation platform, VIT-MBRT, based on a new version 1.2 of *gCTD* [15,16], with potential for reducing

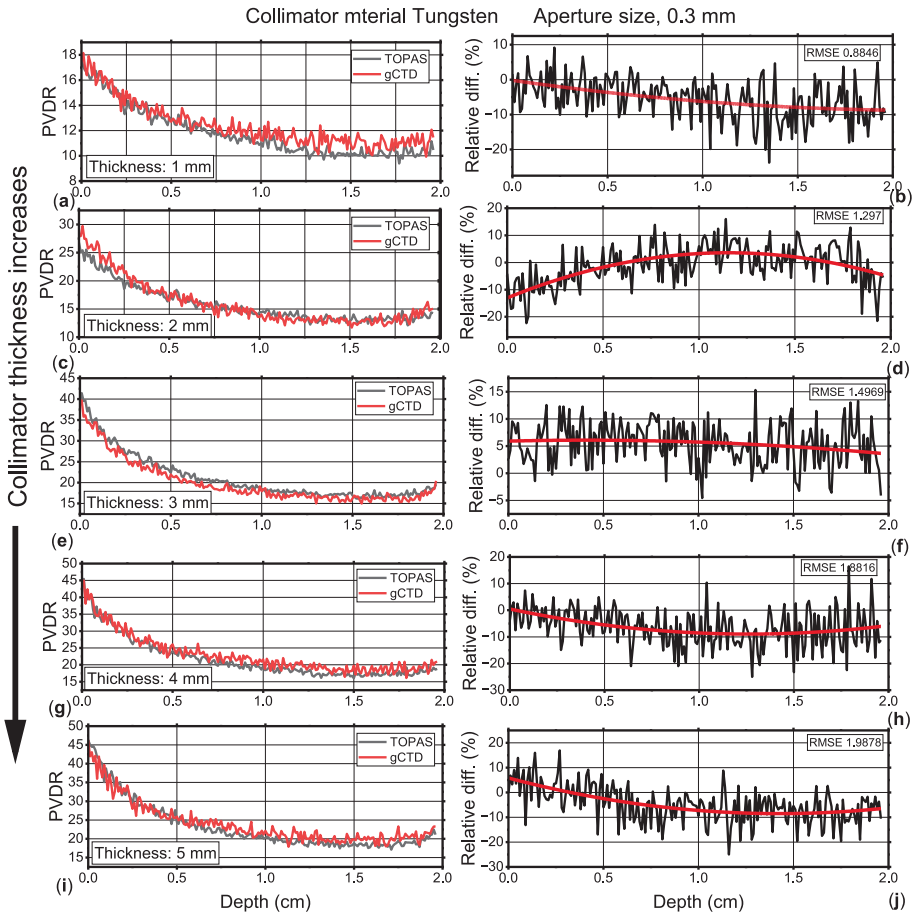

Fig. 12. Comparison of the *PVDR* (left column plots, panels a), c), e), g), i)) at the center of the water cube, when simulating with *TOPAS* and *gCTD* a W/Air multi-slit collimator with a fixed aperture of 0.3 mm and thickness from 1 mm to 5 mm. The right column plots (panels b), d), f), h), j)) show the percentage relative difference for corresponding left-side plots; the continuous red line shows a moving average smoothed trend of the data shown by the continuous black line. (For interpretation of the references to colour in this figure legend, the reader is referred to the web version of this article.)

simulation time for MBRT preclinical treatments to real-time performance (i.e., preclinical 3D dose maps calculated in about the same time as the kilovoltage MBRT physical irradiation of a mouse). To evaluate the accuracy of data generated by this platform, we compared it with a well-validated CPU-based code (*TOPAS*) adopted in published studies [12–14]. For this purpose, we performed several case studies with both codes (*TOPAS* and *gCTD*) under nearly identical geometrical conditions. The first tests involved beam characterization, i.e., the determination of the beam HVL and the mass attenuation coefficient for tungsten, a commonly used material for the collimator's manufacturing in MBRT. The tests showed a good agreement between the simulated and calculated HVL values (Tab. 1) and a relative difference of only 1.5% between the simulated and the expected value of the mass attenuation coefficient of tungsten.

We also investigated the compared performance of the two codes using monoenergetic beams at the average (85 keV) and maximum photon energy (225 keV) of the orthovoltage X-ray spectrum of the preclinical irradiator here adopted. A comparison between the simulated PDD in a $2 \times 2 \times 2$ cm^3 water cube with the two codes showed a relative difference of 0.25% and 0.1% for the beam at 85 and 225 keV, respectively. A relative difference of 0.06% was measured in the case the polychromatic irradiator spectrum was used.

For the minibeam treatment, the dose distribution was simulated in a water phantom, by varying the collimator slit aperture at fixed collimator thickness, and then by varying the collimator thickness at fixed slit aperture. Relative differences between the two codes were in the order of a few percent, but for 0.1 mm and 0.3 mm slit apertures (5-mm thick W collimator) *gCTD* estimates for the depth dose can deviate from the values of *TOPAS* up to 13% at the entrance surface of the beam in the water phantom (Fig. 11a,b and Fig. 12i,j). This peculiar phenomenon might be traced back to the electron tracking capability of *TOPAS* vs. the event local kinetic energy deposition approximated in *gCTD*. In this respect, we are investigating possible photon beam contamination by energetic secondary electrons exiting the tips of the MBRT collimator blades. These electrons may reach the nearby entrance surface of the phantom and deposit energy in the shallowest material layers, a phenomenon which cannot be simulated in *gCTD*. In future work we plan to investigate such aspects of the physical interaction of the incident divergent orthovoltage beam within a tungsten collimator material, with high-resolution full-MC simulations and consideration of electron and fluorescence photon tracking outside the collimator surface and in a close material target.

As shown in Fig. 9b, a dose reduction can be noticed at the entrance and exit surfaces of the phantom in the valley region, consistent with the trends reported by Dipuglia et al. [25]. In their work, using a $14 \times 10 \times 10$ cm^3 phantom, dose reductions were observed within the first 20 mm and in the exit surface of the phantom. We observed a similar trend but limited to the first 10 mm, likely due to the smaller phantom dimensions ($2 \times 2 \times 2$ cm^3), where radiation traversed a shorter path in the material. This effect is attributed to a reduced number of incident photons between slits and to lower scatter contributions at the air–water and water–air interfaces [27]. Consequently, the *PVDR* is higher at the phantom exit (as an example see Fig. 11).

Further evidence supporting the reliability of the *gCTD* code came

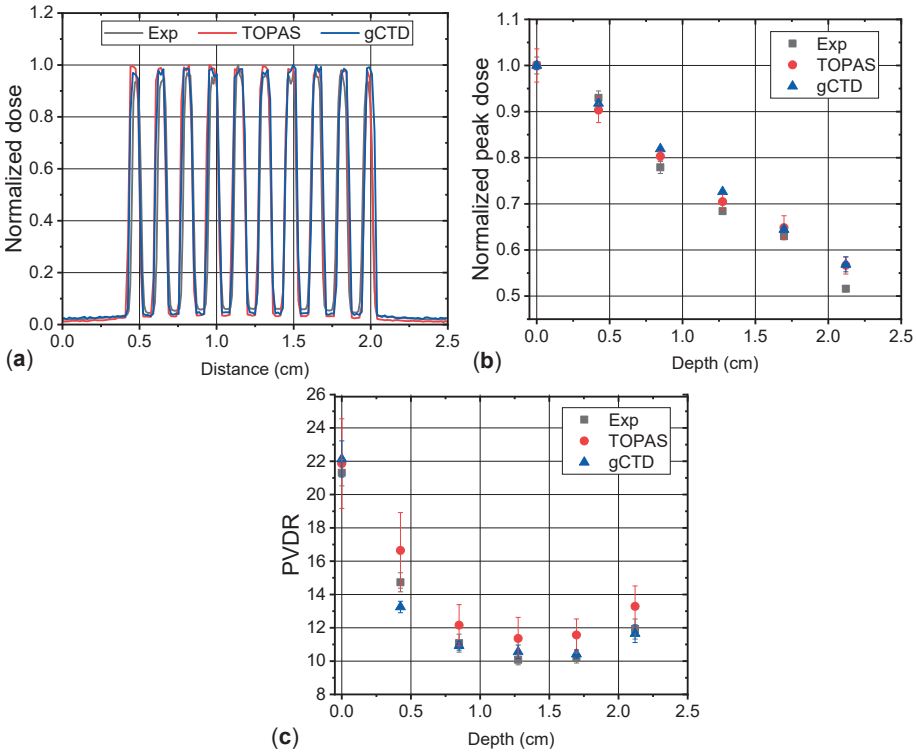

Fig. 13. Comparison of dose profiles (a), peak dose (b) and *PVDR* values through depth (c) between experimental and simulated data.

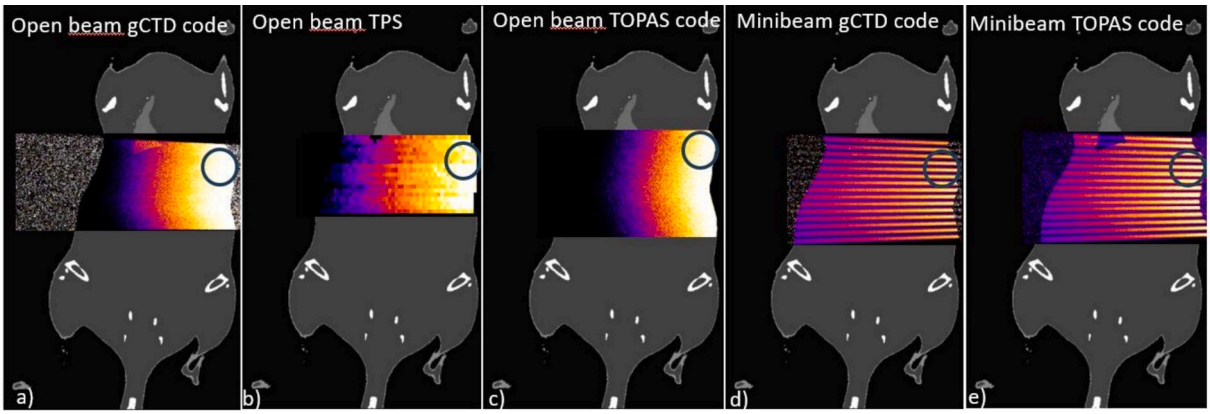

Fig. 14. Dose distribution obtained in the case of mouse in a) an open beam geometry with *gCTD* code, b) with real mouse TPS, and c) *TOPAS* code or with a 5-mm-thick tungsten parallel collimator with an aperture of 0.5 mm d) with *gCTD* code and e) *TOPAS* code. The location of the spherical tumour target is indicated by a circle in these 2D slice dose maps.

from the comparison of absorbed dose measurements in a PMMA phantom. Good agreement was found between experimental and simulated data, with an average relative difference of 2%. This discrepancy can be due to the uncertainty associated with the measured dose values but can also be attributed to the simulated air material in the MBRT slits of the W collimator with respect to the material (polypropylene, density 0.9 g/cm^3) effectively present in the physical W collimator adopted. The *PVDR* calculated in this setup also showed very good agreement, with an average relative difference of 0.5%. It should be noted, however, that the measured differences between the *PVDR* values obtained using the two different codes and from comparison with experimental measurements are subject to statistical fluctuations resulting from the use of a limited number of photons due to the long simulation times required by the *TOPAS* code.

Finally, after the code validation, we tested the *gCTD* code on a mouse phantom reconstructed from a real CT scan provided by San Raffaele Hospital, in Milan. The mouse was irradiated with both open and minibeam treatment using a 5 mm-thick tungsten collimator with a 0.5 mm aperture. A total of 10^{10} photons were simulated. DVHs of the tumour obtained from the open-beam simulation were compared with the real data provided by the TPS of the clinical irradiatior, showing a good agreement (Fig. 15a). The slight discrepancy between the two curves may be due to the different spatial sampling/resolution between the two codes. TPS dose distribution has larger voxel sizes with respect to *gCTD* MC dose distributions. The minibeam simulation was also compared with the corresponding *TOPAS* simulation, again showing good agreement, with a relative difference of 6% (Fig. 15b). In this figure we noted an average dose less than conventional irradiation configurations (Fig. 15a). This effect is consistent with the spatial modulation of the beam which determines a decrease of the average volume dose with respect to open beam irradiation.

The absorbed dose in several mouse organs was also evaluated using

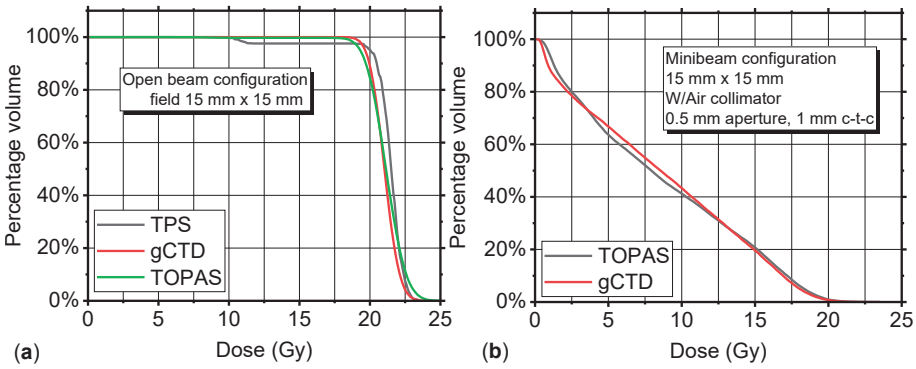

Fig. 15. Comparison of dose-volume histograms in tumour of a mouse irradiated with an open beam, simulated with *gCTD* and *TOPAS*, and derived from the preclinical TPS, (a) and with a parallel-slit W collimator with 0.5 mm slit width and 1 mm c-t-c between *gCTD* and *TOPAS* simulations (b). Irradiated field of view = 15 mm × 15 mm.

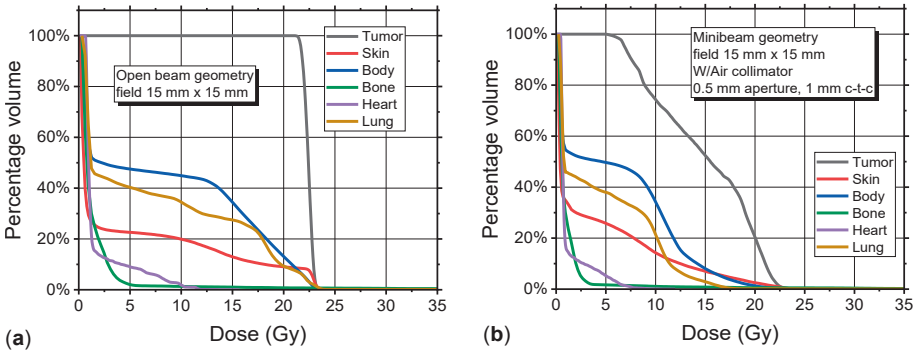

Fig. 16. Dose-volume histograms obtained with *gCTD* code (10^{12} simulated photons) in the several tissues of a mouse irradiated with (a) an open beam field, and (b) a parallel-slit W collimator with 0.5 mm slit width and 1 mm c-t-c. Irradiation field of view = 15 mm × 15 mm. Number of simulated photon histories: 10^{12}.

Table 2
Summary of the software and the computer hardware used for the two codes' simulations, with the relative differences in computation time with different number of primary photons.

Simulation code	Computer hardware	Computing time (s)			Ratio of computing times *TOPAS/gCTD*		
		10^9 photons	10^{10} photons	10^{11} photons	10^9 ph.	10^{10} ph.	10^{11} ph.
TOPAS	2 x AMD EPYC 7281, 2.2 GHz, 32-Core Processors, 256 GB RAM	4512.11	46050.00	305037.00	288	333	298
gCTD v1.2	GPU: NVIDIA GeForce RTX™ 3090Ti	15.66	138.20	1025.01			

gCTD code. For this test, as many as 10^{12} photons were simulated, and DVHs were extracted for organ dose analysis (Fig. 16). The results indicate adequate tumour coverage, with an average dose of 15 Gy in both cases, and a reduced dose to surrounding healty tissues in the minibeam configuration (Fig. 16b). However, the dose remains high for skin and bone, directly exposed to the treatment. It is to be noted that the simulations in mouse phantom were done in a single projection. This study took about 1.9 days computing time.

The virtual studies here shown indicated an overall good agreement between *gCTD* v1.2 and *TOPAS*, but with significant computational time differences (Table 2). We observed that *gCTD* (running on a single GPU card) was about 300 times more computationally efficient than the full-MC code. In *TOPAS*, the total duration of a MC simulation is about 1.2 h, 13 h, and 3.5 d to run 10^9, 10^{10} and 10^{11} primary photons, respectively, and about 16 s, 2 min and 30 min, respectively, with *gCTD* v1.2, with a corresponding relative uncertainty of 0.2%, 0.05% and 0.03% on dose values, respectively. To ensure that all tests be conducted under fair comparison conditions, the hardware used for CPU based tests and that used for GPU based tests were of equivalent commercial value. The *TOPAS* code was run in multithreading mode, utilizing the maximum number of threads supported by the CPU in use. The study in cases 2 and 3 was done with a limited number of photons and therefore a high uncertainty due to the long simulation times of *TOPAS*. We note that the total computing time largely includes data disk saving times: for example, the GPU computing time for *gCTD* was in the order of just 20 s for 10^9 primary photons, this time reducing to one half on last-generation GPUs that we are testing (NVIDIA GeForce RTX 5080, data not shown).

5. Conclusions

We validated an accurate and fast GPU-based MC code (*gCTD* v1.2) as the simulation tool of a platform (VIT-MBRT) for *in silico* reproduction of preclinical MBRT treatments. The validation was done using a CPU-based full-MC code (*TOPAS*) as benchmark, previously validated by our group against MBRT experiments. The *gCTD* code, running on a single high-performance GPU, produces simulations with statistical uncertainty of 0.2% in 16s computing time, with a reduction by about a factor 300 with respect to comparable TOPAS calculations on a CPU-based server. Based on this work, an MC-based preclinical treatment

planning system for the X-RAD225Cx irradiator will be developed within the VIT-MBRT virtual imaging and dosimetry platform.

Declaration of competing interest

The authors declare the following financial interests/personal relationships which may be considered as potential competing interests: G. Mettivier, N. Longo, U. Crimaldi, R. Pacelli, A. Spinelli, C. Fiorino reports financial support was provided by Italian Ministry of Health. G. Mettivier, L.A. Cerbone, P. Russo reports financial support was provided by National Institute of Nuclear Physics (INFN). G. Mettivier, Associate Editor, P. Russo, Past Editor, C. Fiorino, Deputy Editor, given their role as menber of Editorial Board, had no involvement in the peer review of this article and had no access to information regarding its peer review. Full responsibility for the editorial process for this article was delegated to another journal editor. The other authors, they declare that they have no known competing financial interests or personal relationships that could have appeared to influence the work reported in this paper.

Acknowledgements

This work was funded by the European Union - Next Generation EU - NRRP M6C2 - Investment 2.1 Enhancement and strengthening of biomedical research in the NHS, Codice progetto: PNRR-POC-2022-12376062, CUP master: C43C22001370007.All simulations were carried out using the CPU-based and the GPU-accelerated resources of INFN (Istituto Nazionale di Fisica Nucleare), Italy. This work contributes also to the project VITA (Virtual Imaging TriAls) funded by INFN.

Appendix A. Supplementary data

Supplementary data to this article can be found online at https://doi.org/10.1016/j.ejmp.2026.105859.

References

[1] Kraus KM, Winter J, Zhang Y, Ahmed M, Combs SE, Wilkens JJ, et al. *Treatment planning study for microbeam radiotherapy using clinical patient data.* Cancers 2022;14:685.
[2] Slatkin DN, Spanne P, Dilmanian FA, Sandborg M. *Microbeam radiation therapy.* Med Phys 1992;19:1395–400.
[3] Donzelli A., Bräuer-Krisch E., Nemoz C., Brochard T., Oelfke U., *"Conformal image-guided microbeam radiation therapy at the ESRF biomedical beamline ID17"*, Med. Phys. 43, 6(1), 2016, 3157– 67. https://doi.org/10.1118/1.4950724.
[4] Pelliccia D, Poole CM, Livingstone J, Stevenson AW, Smyth LML, Rogers PAW, et al. *"Image guidance protocol for synchrotron microbeam radiation therapy.* J Synchrotron Rad" 2016;23:566–73. https://doi.org/10.1107/S1600577515022894.
[5] Schreiber EC, Sha X, Chang SX. *Monte Carlo simulation of a compact microbeam radiotherapy system based on carbon nanotube field emission technology.* Med Phys 2012;39(8):4669–78.
[6] Chicilo F, et al. *"Dose profiles and x-ray energy optimization for microbeam radiation therapy by high-dose, high resolution dosimetry using Sm-doped fluoroaluminate glass plates and Monte Carlo transport simulation"* to cite this article. Phys Med Biol 2020;65:075010.
[7] Livingstone J, Stevenson AW, Häusermanna D, Adamb J. *Experimental optimisation of the X-ray energy in microbeam radiation Therapy.* Phys Med 2018;45:156.
[8] Shinohara K, Kondoh T, Nariyama N, Fujita H, Washio M, Aoki Y. *Optimization of x-ray microplanar beam radiation therapy for deep-seated tumours by a simulation study.* J Xray Sci Technol 2014;22:395–406.
[9] Smyth LML, Day LR, Woodford K, Rogers PAW, Crosbie JC, Senthi S. *Identifying optimal clinical scenarios for synchrotron microbeam radiation therapy: a treatment planning study.* Phys Med 2019;60:111–9.
[10] Prezado Y, Fois G, Le Duc G, Bravin A. *Gadolinium dose enhancement studies in microbeam radiation therapy.* Med Phys 2009;36(8):3568–74.
[11] Bartzsch S, Eismann S, Oelfke U. *A preclinical microbeam facility with a conventional x-ray tube.* Med Phys 2016;43(12):6301–638.
[12] Akbas CK, Vurro F, Fiorino C, Cozzarini C, Cavaliere F, Milani P, et al. *Preclinical photon minibeam radiotherapy using a custom collimator: Dosimetry characterization and preliminary in-vivo results on a glioma model.* Phys Med 2024;124:103420–10349.
[13] Marson F, Pizzardi S, Alborghetti L, Vurro F, Lacavalla MA, Fiorino C, et al. *Real-time dose measurement in minibeam radiotherapy using radioluminescence imaging.* Phys Med 2025;130:104894.
[14] Pizzardi S, Alborghetti L, Vurro F, Lacavalla MA, Milani CM, Milani P, et al. *Development of a preclinical X-rays minibeam Monte Carlo treatment planning system.* Sci Rep 2025;15:29926.
[15] Jia X, Yan H, Jiang GX. *Fast monte carlo simulation for patient-specific CT/CBCT imaging dose calculation.* Phys Med Biol 2012;57:577–90.
[16] Jia X, Yan H, Cervino L, Jiang FM. *A GPU tool for efficient accurate and realistic simulation of cone-beam CT projections.* Med Phys 2012;39:7368–78.
[17] Cerbone LA, Mettivier G, Lai Y, Jia X, Boyd SK, Russo P. *Absorbed and effective dose estimates in HR-pQCT of the distal radius and tibia: virtual dosimetry with a GPU-accelerated Monte Carlo code.* Phys Med Biol 2025;70.
[18] Woodcock E., Murphy T., Hemmings P. and Longworth S. *"Techniques used in the GEM code for Monte Carlo neutronics calculations in reactors and other systems of complex geometry. In: Applications of Computing Methods to Reactor Problems"*, Argonne National Laboratories Report, 1965, pp 40 ANL-7050.
[19] Berger, M.J., Coursey, J.S., Zucker, M.A., and Chang, J. (2005), "ESTAR, PSTAR, and ASTAR: Computer Programs for Calculating Stopping-Power and Range Tables for Electrons, Protons, and Helium Ions (version 1.2.3)". [Online] Available: http://physics.nist.gov/Star, 2025, National Institute of Standards and Technology, Gaithersburg, MD.
[20] Mettivier G, et al. *Virtual dosimetry study with three cone-beam breast computed tomography scanners using a fast GPU-based Monte Carlo code.* Phys Med Biol 2024;69:045028.
[21] Mettivier G, Sarno A, Lai Y, Golosio B, Fanti V, Italiano ME, et al. *Virtual clinical trials in 2D and 3D X-ray breast imaging and dosimetry: comparison of CPU-based and GPU-based Monte Carlo codes.* Cancers 2022;14(4):1027. https://doi.org/10.3390/cancers14041027.
[22] Perl J, Shin J, Schumann J, Faddegon B, Paganetti H, et al. *TOPAS: an innovative proton Monte Carlo platform for research and clinical applications.* Med Phys 2012;39(11):6818–37.
[23] Poludniowski G, Landry G, DeBlois F, et al. SpekCalc: a program to calculate photon spectra from tungsten anode x-ray tubes. Phys Med Biol 2009;54:N433–8. https://doi.org/10.1088/0031-9155/54/19/N01.
[24] Walters BRB, Kawrakow I, Rogers DWO. *History by history statistical estimators in the BEAM code system.* Med Phys 2002;29(12):2745–52.
[25] Schneider C, Rasband W, Eliceiri K. *NIH image to ImageJ: 25 years of image analysis.* Nat Methods 2012;9:671–5.
[26] Hubbell JH, Seltzer SM. Tables of X-ray mass attenuation coefficients and mass energy-absorption coefficients from 1 keV to 20 MeV for elements Z = 1 to 92 and 48 additional substances of dosimetric interest. Radiation Physics Division, PML, NIST 1996;1989:1990. https://doi.org/10.18434/T4D01F.
[27] Dipuglia A, Cameron M, Davis JA, Cornelius IM, Stevenson AW, Rosenfeld ABF, et al. *Validation of a Monte Carlo simulation for microbeam radiation therapy on the imaging and medical beamline at the Australian synchrotron.* Sci Rep 2019;9:17696–710.